*Progress In Electromagnetics Research M, Vol. 95, 155–163, 2020*

# A Novel Single-Layer Anisotropic Unit for Transmit-Reflect Double Function Array

**Huifen Huang*** **and Shuai-Nan Li**

**Abstract**—In this paper, a novel single-layer anisotropic unit with both reflection and transmission functions is proposed. The unit is a ring-encircled two mirror-symmetry fan-shaped patches, and is fabricated in one side of an F4B substrate. The unit structure is asymmetry with respect to x- and y-axes, and both transmitted and reflected cross-polarized fields are generated simultaneously when the co-polarized field is incident on the symmetry broken surface. Full 360° phase shift range is achieved by utilizing the cross-polarized field, and the transmitted and reflected coefficient magnitudes are above 0.49 close to the theoretical limit. Using this anisotropic unit, three single-layer transmit-reflect-arrays are designed: (1) Two high-gain beams in ($\theta_1 = 0°$, $\varphi_1 = 0°$) and ($\theta_1 = 180°$, $\varphi_1 = 0°$) directions. The gain is 20.9 dBi, and the 3 dB beam width is 8.9°. (2) Two OAM beams with $l = 1$ at ($\theta_1 = 45°$, $\varphi_1 = 0°$) and ($\theta_2 = 135°$, $\varphi_2 = 0°$). (3) Four OAM beams with $l = 1$ at ($\theta_1 = 30°$, $\varphi_1 = 0°$), ($\theta_2 = -30°$, $\varphi_2 = 180°$), ($\theta_3 = 150°$, $\varphi_3 = 0°$) and ($\theta_4 = -150°$, $\varphi_4 = 180°$). The simulated and measured results agree well and validate the design principle. The proposed metasurface has the following advantages: single-layer, transmission and reflection dual-functions, multi-beam, and high gain.

## 1. INTRODUCTION

In 1992, Allen et al. [1] first demonstrated by experiment that a light beam with helical wave front carries orbital angular momentum (OAM). Since then, OAM vortex waves have aroused tremendous interest in biomedicine, optical imaging, atomic physics, and communication field [2–8]. OAM can enhance information transmission rate and capacity over the existing systems because each OAM mode can serve as an independent information channel for the coding, transmission, and reception [9]. In 2007, Thidé et al. [10] proved by numerical simulation that OAM beams can he generated in microwave filed. To generate OAM vortex waves, there are several approaches to produce $e^{il\varphi}$ in microwave frequency. Phased array antennas (usually circular arrays) were utilized for the generation of OAM radiation [6]. Other techniques such as spiral phase plate (SPP) [7], circular traveling-wave antenna [11], dielectric resonator antenna [12], substrate integrated cavity resonator antenna [13], and planar metasurface [14] have also been employed. The circular array antennas usually used complex feeding network, and the gain is low owing to the loss of complicated feeding circuits. The SPP is usually difficult to manufacture. The dielectric resonator antennas and substrate integrated cavity resonator antennas usually have relatively low gains and are difficult to excite high OAM modes.

Metasurfaces are extraordinarily promising in antenna designs because of their low profiles, high gains, and remarkable capability of modulating EM waves [15–17]. In the design of a reflectarray, the antenna is usually composed of units printed on a substrate with single layer and metal ground. The units are used to modulate phase, and the ground is used to reach high reflection coefficient. In the

*Received 11 July 2020, Accepted 6 August 2020, Scheduled 19 August 2020*

* Corresponding author: Huifen Huang (huanghf@scut.edu.cn).

The authors are with the School of Electronic and Information Engineering, South China University of Technology, Guangzhou 510641, China.

design of transmitarray, the antennas usually use stacked units printed on a substrate with a multi-layer structure in order to reach 360° phase shift and high transmission coefficient. However, most of the designed metasurface units can only realize the reflection function or transmission function, and multilayers are needed for realizing both reflection function and transmission simultaneously, which will increase the total thickness, weight, and cost. Metasurfaces have distinctive advantages of versatile radiation characteristics, high gain, easy-to-fabricate, etc., so this paper develops a novel anisotropic single layer unit for designing a multifunction OAM metasurface antenna which can achieve reflection and transmission simultaneously using a single aperture. It has the following advantage: single-layer, multifunction, multi-beam, transmission-reflection double-function, and high gain.

## 2. DESIGN THEORY

### 2.1. Transmit-Reflect Mechanism Based on Cross-Polarization

The schematic for a single-layer metasurface with definitions of transmitted and reflected electric field parameters is shown in Fig. 1. The incident wave is denoted as Ei, and the co- and cross-polarized reflected and transmitted fields are defined as $E_{rc}$, $E_{rx}$, $E_{tc}$, $E_{tx}$, respectively. According to the reference [18], there exists the phase discontinuity limit for both co- and cross-polarized fields for a single-layer surface. If the surface geometry is symmetric with respect to the polarization direction of the incident wave, no cross-polarized field will be excited. The phase angle of co-polarized transmission phase ($\phi c$) is limited within [−90°, 90°]. Furthermore, if a certain co-polarized transmission magnitude ($Tc$) is desired, $\phi c$ will be further reduced. For example, if $Tc \geq 0.5$ (−6 dB) is required, the phase range of $\phi c$ is only [−60°, 60°], and it is drastically reduced to [−45°, 45°] for a −3 dB transmission magnitude requirement. An effective way is to stack multiple layers to obtain full 360° phase coverage. If the surface geometry is symmetry broken, then the cross-polarized field exists, and the magnitude of the cross-polarized reflective and transmission coefficients $|R_X||T_X|$ reach their maximum value 0.5. Furthermore, the phase of cross-polarized $\phi x$ has no limitation. Hence, the full 360° phase range of $\phi x$ can be obtained. Due to the continuity of the cross-polarized field, the same phenomenon is observed for reflective waves. In summary, the phase discontinuity limit of a single-layer EM surface is revealed in this section. For co-polarized field, the phase discontinuity is limited with [−90°, 90°]. For symmetry broken surface, there exist cross-polarized fields, and the full 360° phase range can be achieved for both transmission and reflection simultaneously.

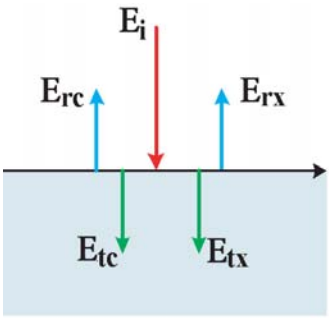


**Figure 1.** Schematic for a single-layer matasurface with definitions of transmitted and reflected electric field parameters.

### 2.2. Design Mechanism for Multifunction OAM Array Antenna

The proposed OAM antenna is shown in Fig. 2, and vectors $u_m$ and $u_n$ are the desired beam directions. It consists of two parts: the horn feeder and metasurface. To generate OAM beam in any designed directions, additional phase-shift $\Delta\varphi_{i,j}$ is compensated by the $(i, j)$th unit in the metasurface to the incident wave.

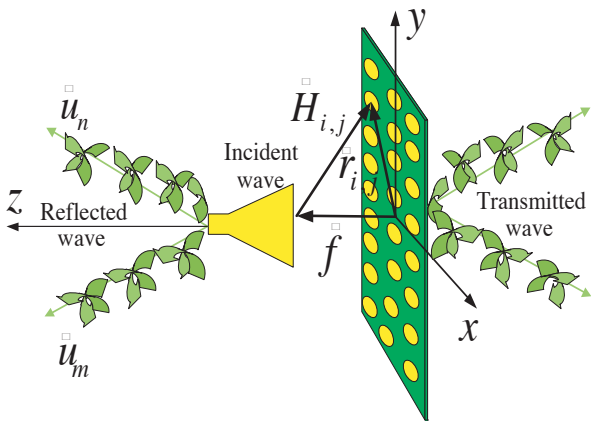


**Figure 2.** The schematic of transmit-reflect-array for generating vortex wave.

The phase of wave front will increase $2\pi l$ after a circle around the center of the metasurface. To get such a spiral phase, the spherical wave of the horn antenna is transferred to the plane wave at first, as in Eq. (1):

$$\Delta\varphi_{1(i,j)} = \frac{2\pi}{\lambda_0} H_{i,j} \tag{1}$$

where $H_{i,j}$ is the distance between the phase center of the horn, and the $(i,j)$th unit cell at the position $(x_i, y_j)$, and $\lambda_0$ is the wavelength in vacuum.

Second, around the center of the array, each unit of the array is given an additional phase shift to obtain spiral phase wavefront as in Eq. (2) for one beam case:

$$\Delta\varphi_{2(i,j)} = \frac{2\pi}{\lambda} \vec{r}_{i,j} \cdot \vec{u}_0 + l \times \tan^{-1}\left(\frac{y_j}{x_i}\right) \tag{2}$$

where $\vec{r}_{i,j} = (x_i, y_j, 0)$ is the position vector of the $(i,j)$th unit cell, and $\vec{u}_0 = (\sin\theta\cos\varphi, \sin\theta\sin\varphi, \cos\theta)$ is the designed OAM beam direction. Therefore, for generating one beam, the total required phase for each unit cell is in Eq. (3):

$$\Delta\varphi_{i,j} = \Delta\varphi_{1(i,j)} + \Delta\varphi_{2(i,j)} = \frac{2\pi}{\lambda_0} H_{i,j} + \frac{2\pi \mathrm{r}}{\lambda} \vec{r}_{i,j} \cdot \vec{u}_0 + l \times \tan^{-1}\left(\frac{y_j}{x_i}\right) \tag{3}$$

To further generate $n$ independent OAM beams, the additional compensation phase $\Delta\varphi_{i,j}$ to obtain spiral phase wavefront is the superposition of $n$ beams as in Eq. (4) [19]:

$$\Delta\varphi_{i,j} = \arg\left\{\sum_{\vec{u}_m}^{\vec{u}_n} \exp\left[j \cdot \left(\frac{2\pi}{\lambda} \vec{r}_{i,j} \cdot \vec{u}_m + l_m \times \tan^{-1}\left(\frac{y_j}{x_i}\right)\right]\right\}\right. \tag{4}$$

where $\vec{u}_m = (\sin\theta_m\cos\varphi_m, \sin\theta_m\sin\varphi_m, \cos\theta_m)_i$ is the $m$th beam direction, and $m$ is in the range of $1 \sim n$. Then, the total compensation phase $\varphi(x_i, y_j)$ for each unit to generate $n$ beams is in Eq. (5):

$$\Delta\varphi\left(x_i, y_j\right) = \frac{2\pi}{\lambda} H_{i,j} + \arg\left\{\sum_{\vec{u}_m}^{\vec{u}_n} \exp\left[j \cdot \left(\frac{2\pi}{\lambda} \vec{r}_{i,j} \cdot \vec{u}_m + l_m \times \tan^{-1}\left(\frac{y_j}{x_i}\right)\right]\right\}\right. \tag{5}$$

In addition, a conventional high gain metasurface antenna is obtained if only the former two items in Eq. (5) are compensated as in Eq. (6).

$$\Delta\varphi\left(x_i, y_j\right) = \frac{2\pi}{\lambda} H_{i,j} + \arg\left\{\sum_{\vec{u}_m}^{\vec{u}_n} \exp\left[j \cdot \left(\frac{2\pi}{\lambda} \vec{r}_{i,j} \cdot \vec{u}_m\right)\right]\right\}\right. \tag{6}$$

## 3. ANTENNA DESIGN

### 3.1. Unit Design

According to the above transmit-reflect mechanism, that a single-layer engineered surface is able to obtain the full 360° phase range of both transmitted and reflected fields by utilizing the cross-polarized field component, a novel single-layer anisotropic unit is proposed at 10 GHz to demonstrate this prediction. The designed anisotropic unit is a ring-encircled two mirror-symmetry fan-shaped patches along the $y = x$ plane and is fabricated in one side of an F4B substrate with thickness 0.55 mm and permittivity ($\varepsilon_r$) 2.25. Figs. 3(a), (b) are the designed unit and its mirror structure, respectively, and Fig. 3(c) is the side view. The geometry parameters for the anisotropic unit marked in Fig. 3 are as follows: $D_1 = D_2 = 15$ mm, $H_1 = 0.55$ mm, $R_1 = 7$ mm, $R_2 = 6.5$ mm, $a_1 = 0.8$ mm, $a_2 = 0.3$ mm, $ag_1 = 5° \sim 75°$, $ag_2 = 4°$. The phase shift is adjusted by changing the angle value of $ag_1$.

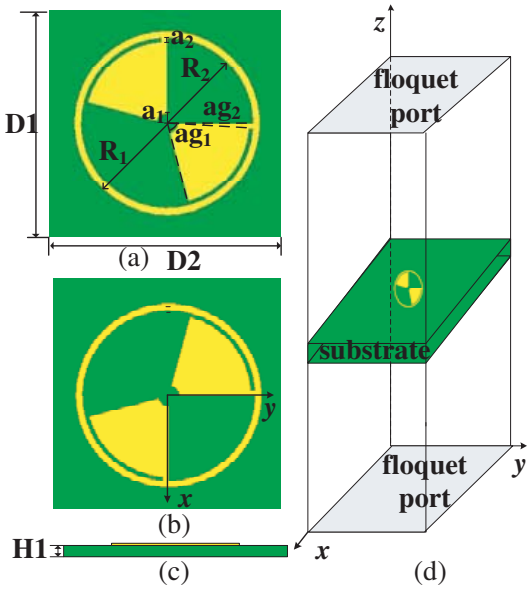


**Figure 3.** Configuration of (a) the proposed anisotropic unit, (b) its mirror structure, (c) side view, and Floquet port simulation model.

The designed units are simulated by HFSS, and the Floquet port simulation model for one of the unit is in Fig. 3(d). The incident wave is $x$-polarized. Fig. 4 shows the simulated phase-shift and $S$ parameter for the designed unit in Fig. 3(a). In the graphic, the former in $P_{i:j}$ ($i, j = 1$, or 2) represents port(i); the latter represents polarization; and $j = 1$ or 2 represents co- or cross-polarization, respectively. $S$ ($p_i$, $p_j$) represents from port(j) to port(i). For example, $S$ ($p1 : 2, p1 : 1$) represents reflective coefficient of the cross-polarization at port 1 under co-polarized incidence wave (here is $x$-polarized). $S$ ($p2 : 2, p1 : 1$) represents transmission coefficient for the cross polarization from port 1 to port 2. The phase shift curve of the unit ranges from 13° to −176°, and all the $S$ parameter amplitudes of the unit are above 0.49 close to the theoretical limit value 0.5. Fig. 5 shows the simulated phase-shift and $S$ parameter for the mirror structure in Fig. 3(b). The phase shift curve of the unit ranges from −171° to −357°, and all the $S$ parameter amplitudes of the mirror unit are above 0.49 close to the theoretical limit value 0.5. The simulated phase shifts show below: (1) The respective phase shifts of Figs. 3(a), (b) are not enough to cover 360°. (2) The phase shift cover more than 360° by combining the phase shifts of two units (anisotropic unit and its mirror structure). Then the phase shift covering more than 360° for reflection and transmission dual functions is achieved by the designed unit and its mirror structure.

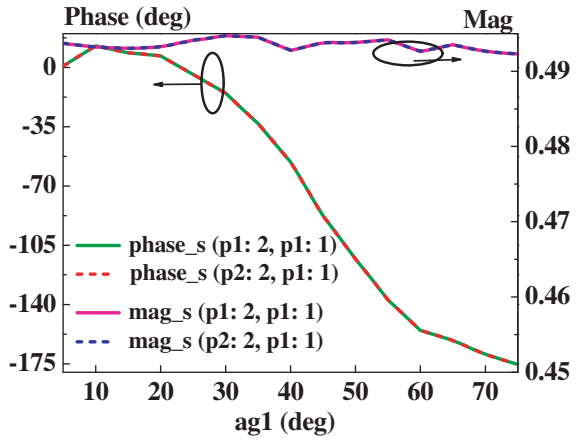


**Figure 4.** The simulated phase shift and $S$ parameter for the designed unit.

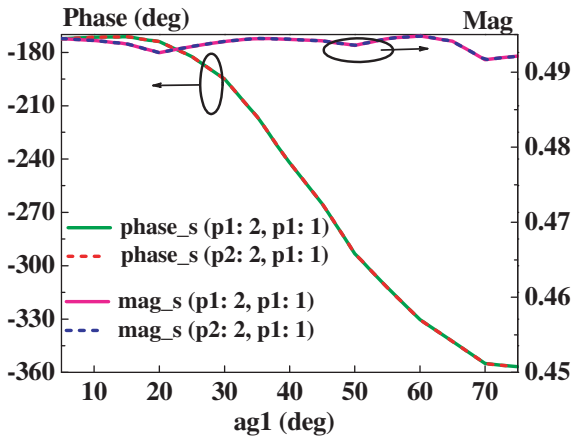


**Figure 5.** The simulated phase shift and $S$ parameter for the design mirror unit.

### 3.2. Design and Analysis of High-Gain Transmit-Reflect-Array

The size of the high-gain transmit-reflect-array made of $16 \times 16$ unit cells is $240 \times 240\,\text{mm}^2$. The phase distributions on the metasurfaces are calculated by MATLAB according to Eq. (6). To generate high-gain beam in ($\theta_1 = 0°$, $\varphi_1 = 0°$) and ($\theta_1 = 180°$, $\varphi_1 = 0°$) directions, the calculated phase is shown in Fig. 6(a). The phase compensation required by the units is matched with the structural variable $ag_1$, and the model is shown in Fig. 6(b).

The radiation pattern has been simulated by CST to verify reflection-transmission double function high gain radiation property. The simulated 3D far-field radiation pattern is shown in Fig. 7. Two symmetric high-gain beams are generated in both sides of the metasurface. The maximum gain of metasurface is 20.9 dBi, and 3 dB beam width is 8.9°.

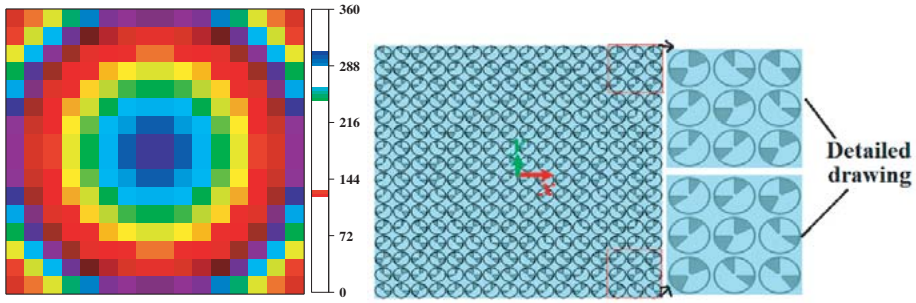


**Figure 6.** The phase distribution of high-gain transmit-reflect-array, (b) the simulated model.

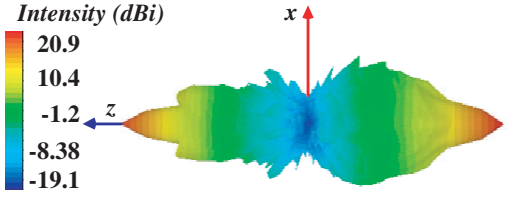


**Figure 7.** The simulated 3D radiation pattern of high-gain transmit-reflect-array.

### 3.3. OAM Transmit-Reflect Multifunction Array

Two single-layer transmit-reflect-arrays are designed. First, two OAM beams with $l = 1$ at ($\theta_1 = 45°$, $\varphi_1 = 0°$) and ($\theta_2 = 135°$, $\varphi_2 = 0°$). The size of the OAM transmit-reflect-array made of 16×16 unit cells is $240 \times 240\,\text{mm}^2$. The phase compensation required for each unit is calculated according to Eq. (3). The phase distribution is shown in Fig. 8(a), and the simulation model is shown in Fig. 8(b). The simulated 3D far-field radiation pattern is shown in Fig. 9, and Figs. 9(a), (b) are the side and top views, respectively. Two symmetric OAM beams with "hollow" characteristics are generated in two sides of metasurface. The reflected OAM beam is generated in ($\theta_1 = 45°$, $\varphi_1 = 0°$) direction, and the transmitted OAM beam is generated in ($\theta_2 = 135°$, $\varphi_1 = 0°$) direction. The peak gain is 13.9 dBi. In addition, a high-gain directional beam is formed along the $z$-axis, which is caused by the co-polarization field.

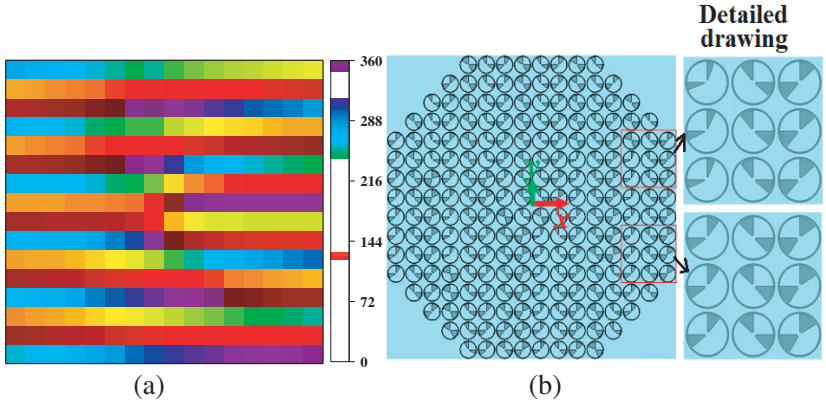


**Figure 8.** The phase distribution of OAM transmit-reflect-arrays with two beams, and (b) the simulated model.

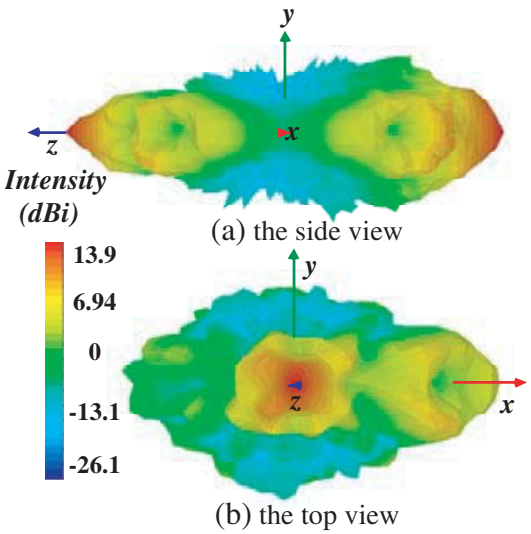


**Figure 9.** The simulated 3D radiation pattern of OAM transmit-reflect-array.

Second, four OAM beams are with $l = 1$ at ($\theta_1 = 30°$, $\varphi_1 = 0°$), ($\theta_2 = -30°$, $\varphi_2 = 180°$), ($\theta_3 = 150°$, $\varphi_3 = 0°$) and ($\theta_4 = -150°$, $\varphi_4 = 180°$) directions. The size of the OAM transmit-reflect-array made of $16 \times 16$ unit cells is $240 \times 240\,\text{mm}^2$. The phase compensation required for each unit is calculated according to Eq. (5). The phase distribution is shown in Fig. 10(a), and the simulation model is shown in Fig. 10(b). The simulated 3D far-field radiation pattern is shown in Fig. 11, and

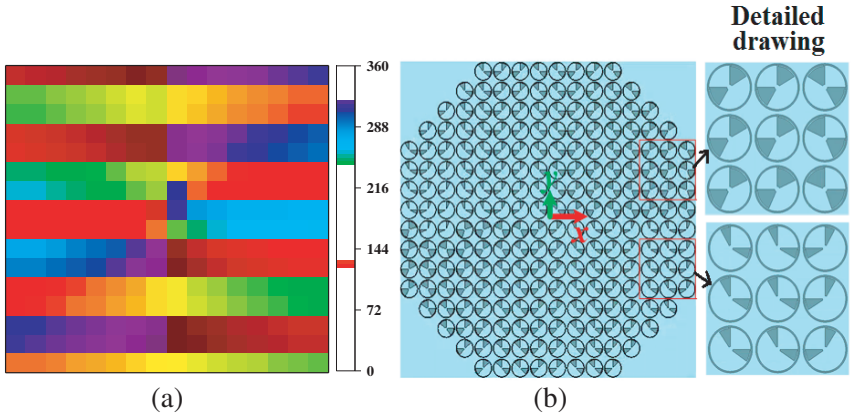


**Figure 10.** (a) The phase distribution of OAM transmit-reflect-arrays with four beams, and (b) the simulated model.

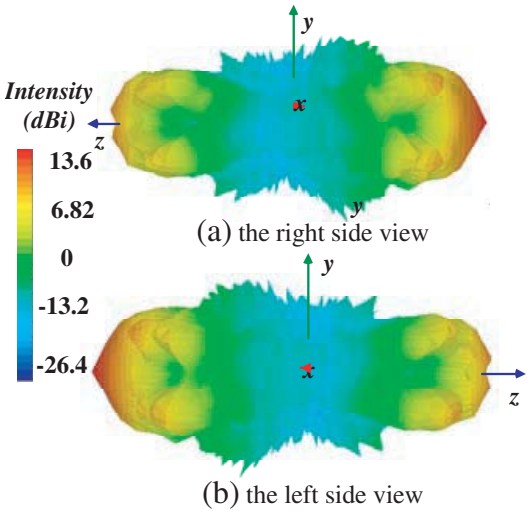


**Figure 11.** The simulated 3D radiation pattern of OAM transmit-reflect-array.

Figs. 11(a), (b) are the right and left side views, respectively. It can be seen that four symmetric OAM beams with "hollow" characteristics are generated in both sides of metasurface. There are two OAM beams in the right (left) side of the array antenna. The reflected OAM beams are in ($\theta_1 = 30°$, $\varphi_1 = 0°$) and ($\theta_2 = -30°$, $\varphi_2 = 180°$) directions, and the transmitted OAM beams are in ($\theta_3 = 150°$, $\varphi_3 = 0°$) and ($\theta_4 = -150°$, $\varphi_4 = 180°$) directions. The peak gain is 13.6 dBi.

## 4. EXPERIMENT RESULTS

In order to validate the design, a prototype for the designed OAM metasurface in Fig. 8 with ($l_1 = 1$, $\theta_1 = 45°$, $\varphi_1 = 0°$) and ($l_2 = 1$, $\theta_2 = 135°$, $\varphi_2 = 0°$) is fabricated and tested. The prototype top view and the test environment are in Fig. 12, respectively.

Figure 13 shows the measured normalized 2D radiation patterns. It can be found that around $\theta = 45°$, the intensity of field reaches its singularity. The simulated and measured results agree well and validate the design principle. However, it is worth pointing out that the aperture efficiency of the bidirectional high gain antenna is inherently low, and there are two reasons. 1) The input energy is divided between co-pol and cross-pol, resulting in 3 dB loss. 2) The cross-pol energy is divided between a transmitted beam and a reflected beam, leading to another 3 dB reduction.

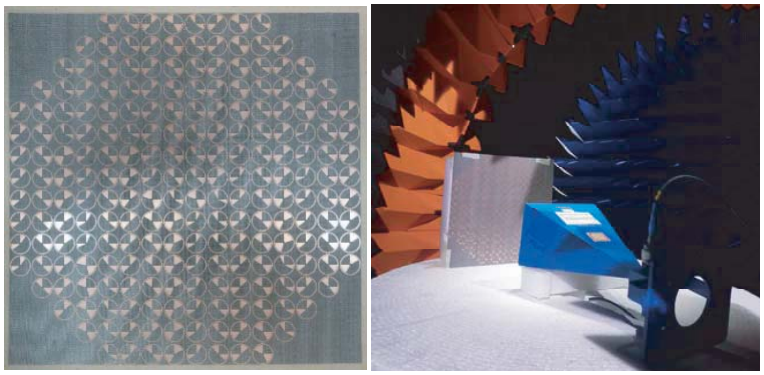

(a) (b)

**Figure 12.** (a) The prototype corresponding to Fig. 8, and (b) test environment.

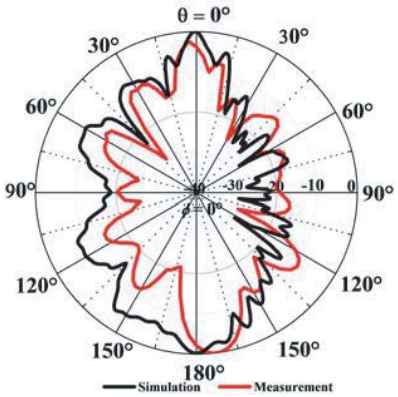


**Figure 13.** The simulation and measured 2D radiation pattern.

## 5. CONCLUSION

This paper proposes a single-layer transmit-reflect double function anisotropic unit. As examples, three single layer transmit-reflect-arrays made of the developed units are designed: (1) High gain directional beams. (2) Two OAM beams with $l = 1$ at ($\theta_1 = 45°$, $\varphi_1 = 0°$) and ($\theta_2 = 135°$, $\varphi_2 = 0°$). (3) Four OAM beams with $l = 1$ at ($\theta_1 = 30°$, $\varphi_1 = 0°$), ($\theta_2 = -30°$, $\varphi_2 = 180°$), ($\theta_3 = 150°$, $\varphi_3 = 0°$) and ($\theta_4 = -150°$, $\varphi_4 = 180°$). The simulated and measured results agree well and prove that the developed unit can be used to simultaneously realize both reflection and transmission dual functions using a single aperture. The proposed metasurface has the following advantage: single-layer, transmission and reflection dual-functions, multi-beams, and high gain.

## ACKNOWLEDGMENT

This work was supported by the Key Project of Natural Science Foundation of Guangdong Province of China under Grant 2018B030311013, the Natural Science Foundation of Guangdong province under Grant 2016A030313462, the National Natural Science Foundation of China under Grant 61071056.

## REFERENCES

1. Allen, L., M. W. Beijersbergen, R. Spreeuw, and J. Woerdman, "Orbital angular momentum of light and the transformation of Laguerre-Gaussian laser modes," *Phys. Rev. A*, Vol. 45, No. 11, 8185, Jun. 1992.

2. Yan, Y., G. Xie, M. P. J. Lavery, et al., "High-capacity millimeter-wave communications with orbital angular momentum multiplexing," *Nature Commun.*, Vol. 5, 4876, 2014.
3. Edfors, O. and A. J. Johansson, "Is orbital angular momentum (OAM) based radio communication an unexploited area?," *IEEE Trans. Antennas Propag.*, Vol. 60, No. 2, 1126–1131, 2012.
4. Zhao, N., X. Li, G. Li, and J. M. Kahn, "Capacity limits of spatially multiplexed free-space communication," *Nature Photon.*, Vol. 9, 822–826, 2015.
5. Chen, M., K. Dholakia, and M. Mazilu, "Is there an optimal basis to maximise optical information transfer?," *Sci. Rep.*, Vol. 6, Art. No. 22821, 2016.
6. Gong, Y. H., R. Wang, and Y. K. Deng, "Generation and transmission of OAM-carring vortex beams using circular antenna array," *IEEE Trans. Antennas Propag.*, Vol. 65, No. 6, 2940–2949, Jun. 2017.
7. Hui, X. N., S. L. Zheng, Y. P. Hu, et al., "Ultralow reflectivity spiral phase plate for generation of millimeter-wave OAM beam," *IEEE Antennas Wireless Propag. Lett.*, Vol. 14, 966–969, 2015.
8. Pan, Y., et al., "Generation of orbital angular momentum radio waves based on dielectric resonator antenna," *IEEE Antennas Wireless Propag. Lett.*, Vol. 16, 385–388, 2017.
9. Yan, Y., G. Xie, M. P. J. Lavery, et al., "High-capacity millimeter-wave communications with orbital angular momentum multiplexing," *Nature Commun.*, Vol. 5, 4876, 2014.
10. Thidé, B., et al., "Utilization of photon orbital angular momentum in the low-frequency radio domain," *Phys. Rev. Lett.*, Vol. 99, No. 8, Art. No. 087701, Aug. 2007.
11. Zhang, Z., S. Zheng, X. Jin, H. Chi, and X. Zhang, "Generation of plane spiral OAM waves using traveling-wave circular slot antenna," *IEEE Antennas Wireless Propag. Lett.*, Vol. 16, 8–11, 2017.
12. Ren, J. and K. W. Leung, "Generation of microwave orbital angular momentum states using hemispherical dielectric resonator antenna," *Appl. Phys. Lett.*, 2018, doi.org/10.1063/1.5021951.
13. Chen, Y., et al., "Half-mode substrate integrated waveguide antenna for generating multiple orbital angular momentum modes," *Electronics Lett.*, Vol. 52, 684–686, 2016.
14. Chen, Y., S. Zhang, Y. Hui, X. Jin, H. Chi, and X. Zhang, "A flat-lensed spiral phase plate based on phase-shifting surface for generation of millimeter-wave OAM beam," *IEEE Antennas Wireless Propag. Lett.*, Vol. 15, 1156–1158, 2016.
15. Qin, F., L. Wan, L. Li, et al., "A transmission metasurface for generating OAM beams," *IEEE Antennas Wireless Propag. Lett.*, Vol. 17, No. 10, 1793–1796, 2018.
16. Chen, M. L. N., L. J. Jiang, and W. E. I. Sha. "Ultrathin complementary metasurface for orbital angular momentum generation at microwave frequencies," *IEEE Trans. Antennas Propag.*, Vol. 65, No. 1, 396–400, 2017.
17. Ma, L., C. Chen, L. Zhou, et al., "Single-layer transmissive metasurface for generating OAM vortex wave with homogeneous radiation based on the principle of Fabry-Perot cavity," *Appl. Phys. Lett.*, Vol. 114, No. 8, 081603, 2019.
18. Yang, F., R. Deng, X. Xu, et al., "Design and experiment of a near-zero-thickness high-gain transmit-reflect-array antenna using anisotropic metasurface," *IEEE Trans. Antennas Propag.*, Vol. 66, No. 6, 2853–2861, 2018.
19. Yu, S. X., L. Li, G. Shi, et al., "Generating multiple orbital angular momentum vortex beams using metasurface in radio frequency domain," *Appl. Phys. Lett.*, Vol. 108, 241901, 2016.